Thylakoid luminal θ-carbonic anhydrase critical for growth and photosynthesis in the marine diatom *Phaeodactylum tricornutum*

Sae Kikutani[a,1], Kensuke Nakajima[a,1], Chikako Nagasato[b], Yoshinori Tsuji[a], Ai Miyatake[a], and Yusuke Matsuda[a,2]

[a]Department of Bioscience, School of Science and Technology, Kwansei Gakuin University, Sanda, Hyogo 669-1337, Japan; and [b]Muroran Marine Station, Field Science Center for Northern Biosphere, Hokkaido University, Muroran, Hokkaido 051-0013, Japan

Edited by Paul G. Falkowski, Rutgers, The State University of New Jersey, New Brunswick, NJ, and approved June 20, 2016 (received for review February 24, 2016)

The algal pyrenoid is a large plastid body, where the majority of the CO_2-fixing enzyme, ribulose-1,5-bisphosphate carboxylase/oxygenase (RubisCO) resides, and it is proposed to be the hub of the algal CO_2-concentrating mechanism (CCM) and CO_2 fixation. The thylakoid membrane is often in close proximity to or penetrates the pyrenoid itself, implying there is a functional cooperation between the pyrenoid and thylakoid. Here, GFP tagging and immunolocalization analyses revealed that a previously unidentified protein, Pt43233, is targeted to the lumen of the pyrenoid-penetrating thylakoid in the marine diatom *Phaeodactylum tricornutum*. The recombinant Pt43233 produced in *Escherichia coli* cells had both carbonic anhydrase (CA) and esterase activities. Furthermore, a Pt43233:GFP-fusion protein immunoprecipitated from *P. tricornutum* cells displayed a greater specific CA activity than detected for the purified recombinant protein. In an RNAi-generated *Pt43233* knockdown mutant grown in atmospheric CO_2 levels, photosynthetic dissolved inorganic carbon (DIC) affinity was decreased and growth was constantly retarded; in contrast, overexpression of Pt43233:GFP yielded a slightly greater photosynthetic DIC affinity. The discovery of a θ-type CA localized to the thylakoid lumen, with an essential role in photosynthetic efficiency and growth, strongly suggests the existence of a common role for the thylakoid-luminal CA with respect to the function of diverse algal pyrenoids.

marine diatom | CGHR domain | luminal carbonic anhydrase | CO_2-concentrating mechanism | pyrenoid

Marine diatoms are major primary producers, which are responsible for up to 20% of annual global carbon fixation (1, 2). To overcome the difficulties of CO_2 limitation in alkaline and high-salinity seawater, diatoms use a CO_2-concentrating mechanism (CCM) for the intracellular accumulation of dissolved inorganic carbon (DIC) (3). It is known that the marine pennate diatom, *Phaeodactylum tricornutum*, uses solute carrier 4 (SLC4) family transporters to take up HCO_3^- actively from the surrounding seawater (4). Based upon physiological measurements of cellular DIC flux, it has been hypothesized that accumulated HCO_3^- is further concentrated in the chloroplast and that an ample flux of CO_2 to ribulose-1,5-bisphosphate carboxylase/oxygenase (RubisCO) is facilitated by the pyrenoidal β-carbonic anhydrases (CAs), PtCA1 and PtCA2 (5, 6). In this process, α-type CAs present in the matrices of the four-layered chloroplast membranes are thought to prevent leakage of CO_2 from the chloroplast in *P. tricornutum* (7, 8).

Algal CCMs are distinct from their carboxysomal counterparts in cyanobacteria, and were most likely acquired by an extensive convergent evolution process (9). It is postulated that the algal CCM is composed of active DIC transport systems at the plasma membrane and the chloroplast envelope, as well as a highly localized CO_2 formation system within close proximity to RubisCO. The possibility remains that the latter process occurs within the pyrenoid, an inner-chloroplastic protein body packed with RubisCO aggregates (10). In the green alga, *Chlamydomonas reinhardtii*, the pyrenoid is considered to be a functional analog of the cyanobacterial carboxysome; the operation of the CCM is synchronous with the formation of the pyrenoid (11). It is postulated that the pyrenoid maintains the accumulated CO_2 in *C. reinhardtii* by preventing CO_2 leakage from the chloroplast through the concerted action of a stromal β-CA, carbonic anhydrase 6 (CAH6), and a low-CO_2–inducible (LCI) B/C protein complex (12, 13). The LCIB/C complex is located at a peripheral region of the pyrenoid under CO_2-limiting conditions in the presence of light. Moreover, impairment of LCIB results in a lethal phenotype under moderate CO_2 limitation but is nonlethal under severe CO_2 limitations, indicating it operates under a specific low-CO_2 range (12). This pyrenoid-based CCM in *C. reinhardtii* also includes enzymes within the thylakoid-invaginating pyrenoid, such as the thylakoid-luminal α-CA, CAH3, an enzyme that could be essential for producing an ample flux of CO_2 to RubisCO by using the acidity of the thylakoid lumen (14, 15). Alternatively, it is also hypothesized that CAH3 can remove a proton from the water-oxidizing complex on the donor side of photosystem II (PSII) by supplying HCO_3^-, thus maintaining an optimal rate of oxygen evolution (16, 17).

Recent studies on secondary symbionts (e.g., marine diatoms) provide evidence for an alternate CCM to the CCM known for the freshwater primary-symbiont *C. reinhardtii*. In *P. tricornutum*, there are a number of putative HCO_3^- transporter genes belonging to the SLC4 and SLC26 families; PtSLC4-2 is a sodium-dependent

Significance

The protein Pt43233 is a member of the Cys-Gly-His–rich (CGHR) protein family, and it was discovered to be a previously unidentified carbonic anhydrase (CA), designated as θ-CA. Moreover, Pt43233 is targeted to the lumen of the pyrenoid-penetrating thylakoid in the marine diatom *Phaeodactylum tricornutum*. Analysis of Pt43233 overexpression and RNAi mutants suggests this CA is essential for photosynthetic efficiency and growth in this diatom. The discovery of θ-CA within the pyrenoid-penetrating thylakoid of *P. tricornutum* implies direct use of the pH gradient across the thylakoid membrane as a means of supplying CO_2 to the Calvin cycle. Alternatively, Pt43233 could regulate the function of photosystems, indicating that a common mechanism could have evolved convergently across diverse aquatic photoautotrophs.

Author contributions: Y.M. designed research; S.K., K.N., C.N., Y.T., and A.M. performed research; S.K., K.N., and Y.M. analyzed data; and S.K., K.N., and Y.M. wrote the paper.

The authors declare no conflict of interest.

This article is a PNAS Direct Submission.

Freely available online through the PNAS open access option.

Data deposition: The sequences reported in this paper have been deposited in the GenBank database (accession nos. LC111565, LC111566, LC111567, and LC111568).

[1]S.K. and K.N. contributed equally to this work.

[2]To whom correspondence should be addressed. Email: yusuke@kwansei.ac.jp.

This article contains supporting information online at www.pnas.org/lookup/suppl/doi:10.1073/pnas.1603112113/-/DCSupplemental.

HCO_3^- transporter at the plasma membrane (4). There are nine CA genes present within the *P. tricornutum* genome; five are α-type CAs localized in the matrices of the four-layered plastid membranes, two are β-CAs located in the pyrenoid, and two are mitochondrial γ-CAs (8). By contrast, *P. tricornutum* CAs are not known to occur in the thylakoid lumen, although pyrenoidal (not stromal) β-CAs, PtCA1 and PtCA2, have been described (8). Taken together, it is suggested that there are differences in the control of DIC flux at the pyrenoid in diatoms relative to *C. reinhardtii*.

In the present study, we provide evidence that *P. tricornutum* contains a previously unidentified CA, herein designated as a θ-CA. This θ-CA is found in the lumen of the pyrenoid-penetrating thylakoid and appears to be critical for photosynthetic efficiency and growth in the marine diatom *P. tricornutum*.

Results

The Cys-Gly-His–Rich Family in Diatoms. Putative orthologs of the *C. reinhardtii* LCIB protein are widely distributed in bacteria, chlorophyta, glaucophyta, and heterokontophyta (12), and are divided into four distinct clades in this study on the basis of dissimilarity at the overall amino acid sequence level (Fig. S1). However, these orthologs contain a domain with highly conserved amino acids, CDGAHPHGRCG, within a sequence length of ∼110 amino acids (Fig. 1). Henceforth, this domain is referred to as the Cys-Gly-His–rich (CGHR) domain.

The *P. tricornutum* genome contains four genes within the CGHR family that are clustered together on chromosome 1, specifically *Pt43234*, *Pt43233*, *Pt43232*, and *Pt32401*; in silico translations of these gene sequences revealed their CGHR domains are well conserved in proteins belonging to distant photoautotrophs (Fig. 1 *A* and *B*). Phylogenetic analysis revealed a similarity of the CGHR family proteins between diatoms and bacteria. In contrast, the diatom CGHR family was distinct from CGHR family proteins in cyanobacteria and green algae (Fig. S1). The *P. tricornutum* CGHR family contains diversely arranged CGHR domains (Fig. 1*C*). Pt43233 and Pt43234 each possess one CGHR domain, which is located at the central portion and N terminus of the polypeptide, respectively, whereas both Pt43232 and Pt32401 possess two CGHR domains and are 95% identical at the amino acid level. An in silico analysis of the four CGHR proteins revealed an absence of subcellular targeting signals for Pt43232, Pt43234, and Pt32401 (Fig. 1*C*). In addition, all four CGHR proteins did not possess membrane-spanning helices. The N-terminal transit peptide sequence in Pt43233 consisted of an endoplasmic reticulum (ER) signal and a plastid-transit sequence (TAA-FQT) at the predicted cleavage site of the ER signal (Fig. S2*A*), corresponding to one of the variants of the ASA-FAP motif (18). Moreover, the Pt43233 sequence contained the thylakoid-targeting domain (TTD) (19) (Fig. 1*C* and Fig. S2*A*). Thereafter, our primary focus was the biochemical and functional characterization of the putative chloroplastic CGHR protein, Pt43233.

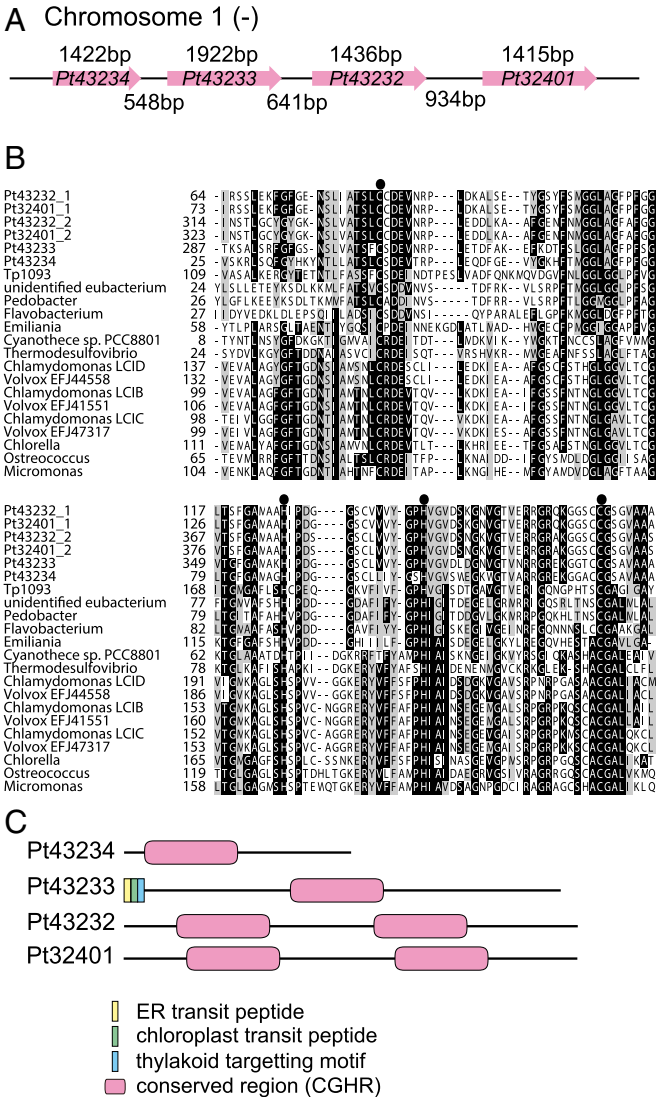

Fig. 1. Structural comparison of CGHR family members in the *P. tricornutum* genome and conserved regions in CGHR family proteins from other photoautotrophs. (*A*) Schematic drawing of *P. tricornutum* CGHR family genes on chromosome 1. Magenta arrows indicate the cDNA sequence regions for CGHR family genes, and the numbers above the arrows represent their corresponding lengths. The numbers shown below the arrows indicate the length of noncoding regions. (*B*) Comparison of the conserved regions in CGHR family proteins from bacteria, cyanobacteria, and eukaryotic algae. (*C*) Schematic drawings of notable domain structures of four *P. tricornutum* CGHR family members.

Subcellular Localization and Environmental Responses of Pt43233. Subcellular localization of Pt43233 was carried out by expressing a C-terminal GFP-fusion protein in *P. tricornutum*. The fluorescence signal associated with a Pt43233:GFP transformant (clone 1, Pt43233:GFP1) was visible as a rod shape within the center of the chloroplast (Fig. 2 *A*–*D*). Additional analysis of Pt43233:GFP1 subcellular localization was done immunohistochemically using transmission electron microscopy (TEM) and compared with another clone harboring Pt43233:GFP (clone 2, Pt43233:GFP2). For both Pt43233:GFP transformants, the protein was located on the thylakoid membrane structure and within the pyrenoid (Fig. 2 *E* and *F* and Fig. S2*B* for clone 1 and Fig. 2 *G* and *H* for clone 2). This finding is in agreement with the in silico analysis of the N-terminal signal sequence (Fig. 1*C*). A similar analysis with a Pt43233:GFP-fusion protein minus the putative TTD (Pt43233Δ47–67:GFP) (Fig. S2*A*) revealed this protein to be targeted to the stroma (Fig. 2*I*). Stromal targeting was also evident for a deletion mutant of the second alanine-rich region in the TTD (Pt43233Δ55–67:GFP) (Fig. 2*J*). By comparison, fluorescence microscopy revealed that CGHR proteins, Pt43232 and Pt32401, were rod-like in appearance and localized to the extra-chloroplastic space (Fig. S3*A*). TEM confirmed these proteins resided in the mitochondrion or outside of the chloroplast (Fig. S3*B*). Taken together, these data indicate that amino acid residues 47–67 within the N terminus of Pt43233 serve as a TTD and that Pt43233 resides in the lumen of the pyrenoid-penetrating thylakoid. Interestingly, the centric diatom, *Thalassiosira pseudonana*, also possesses a putative CGHR family gene (*Tp1093*), and the deduced amino acid sequence also contains a plastid transit peptide and a TTD (Figs. S1 and S2*A*).

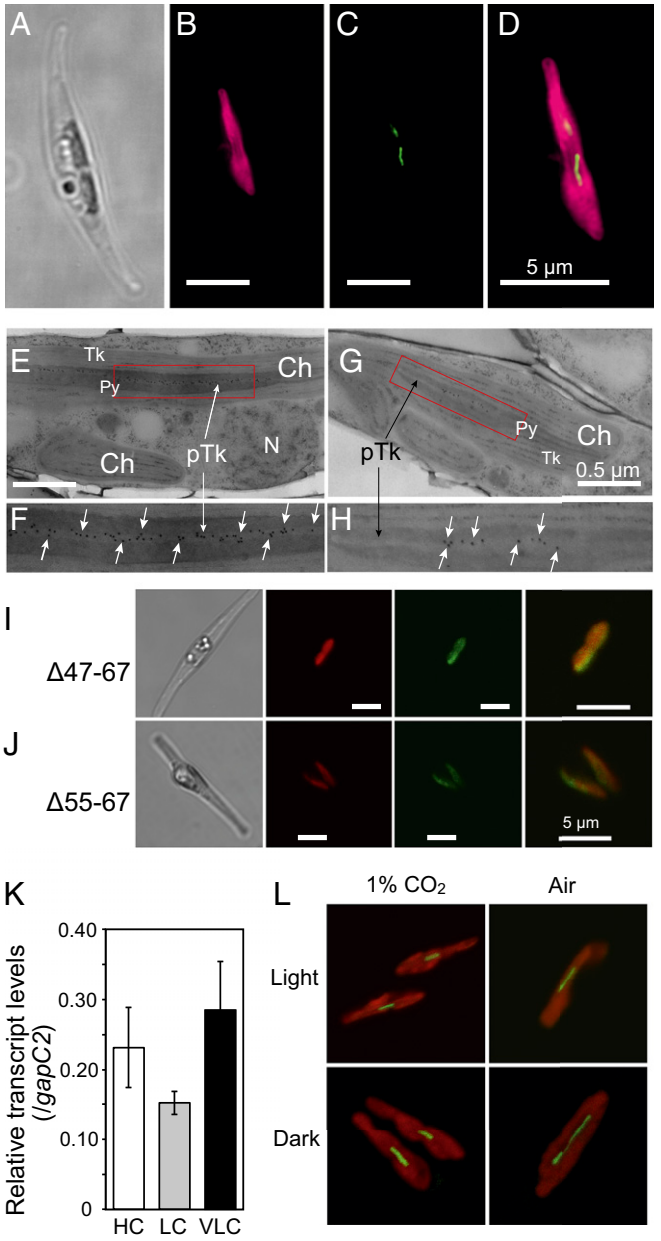

Fig. 2. Subcellular localization and transcript abundance analysis of Pt43233. Superresolution microscopy analysis of Pt43233:GFP localization in a *P. tricornutum* Pt43233:GFP1 mutant: light image (*A*), chlorophyll autofluorescence (*B*, red), GFP fluorescence (*C*, green), and merged image of *B* and *C* (*D*). (Scale bars, 5 μm.) (*E*) Immunogold labeling TEM image of the Pt43233:GFP1 mutant. The Pt43233:GFP1 mutant was subjected to TEM following immunogold labeling with anti-GFP antibody. Representative gold particles are indicated by the white arrows in *E*–*H*. (*F*) Magnification of the box in *E*. (*G*) Immunogold labeling TEM image of the Pt43233:GFP2 mutant. (*H*) Magnification of the box in *G*. (*I* and *J*) Respective subcellular localization analysis of Pt43233Δ47–67:GFP and Pt43233Δ55–67:GFP by laser-scanning confocal microscopy. A light image (*Left*), chlorophyll autofluorescence (*Left Center*), GFP (*Right Center*), and merged image (*Right*) are shown. (Scale bars, 5 μm.) (*K*) Quantitative RT-PCR analysis of changes in transcript levels in response to changing CO_2 conditions. *Pt43233* transcript levels in *P. tricornutum* cells cultured under 5% (vol/vol) CO_2 (HC), atmospheric air (LC), or very low CO_2 (VLC; <0.002%) with continuous illumination. The *gapC2* gene was used as the internal standard. The error bars indicate SDs of three separate experiments. (*L*) Localization analysis of Pt43233:GFP in Pt43233:GFP2 mutant grown under 1% CO_2 (1%) and 0.04% CO_2 (Air) under light and dark conditions.

Transcript levels of endogenous Pt43233 were not altered in response to varying CO_2 levels, including cells cultured under high (1% CO_2), atmospheric air (0.04% CO_2), and very low (<0.002% CO_2) CO_2, indicating that this protein is not transcriptionally regulated by CO_2 (Fig. 2*K*). Subcellular localization of an exogenous Pt43233:GFP fusion in Pt43233:GFP2 cells was not altered by growth under a range of CO_2/light conditions (Fig. 2*L*), implying that Pt43233 is a constitutive thylakoid-luminal factor specifically localized at the pyrenoid-penetrating thylakoid. Structural details of the pyrenoid-containing chloroplast with thylakoid membranes are illustrated in Fig. S2*B*. Localization and transcriptional responses of all CGHR factors are listed in Figs. S3 and S4.

Pt43233 as a θ-Type CA. The CGHR domain contains a well-conserved sequence (Fig. 1*B*) with C, D, and H amino acid residues, forming a putative divalent cation-chelating moiety, which is a prominent feature in CA and zinc-finger proteins (20). In fact, the purified recombinant Pt43233 (Fig. S5*A*) contained a Zn/protein molar ratio of 1.43 ± 0.4, which was about 14-fold greater than the Zn/protein molar ratio of cytochrome *c* (0.10 ± 0.04 mol·mol^{-1} protein), a non-Zn chelating metalloprotein (Table S1). Indeed, the purified recombinant Pt43233 had CO_2 hydration [30.9 ± 0.8 Wilbur–Anderson unit (WAU)·mg^{-1} protein] and HCO_3^- dehydration (42.2 ± 0.8 WAU·mg^{-1} protein) activities (Table S1). The recombinant Pt43233 was further treated with 1 mM EDTA to chelate Zn^{2+}, followed by dialysis with a Zn^{2+}-free buffer. The CA activity of the Zn-free Pt43233 preparation was reduced by 33% relative to the Zn-containing Pt43233 (Fig. 3*A*), confirming that Zn is required for optimal CA activity in Pt43233.

To confirm the occurrence of CA in vivo, cell lysate of the Pt43233:GFP overexpressing transformant (clone 1) was assayed for CA activity. Total CO_2 hydration activity at pH 8.0–8.3 was marginal in cell lysate prepared from 1% CO_2-grown wild-type (WT) cells, whereas the HCO_3^- dehydration rate at pH 5.7–6.0 was ∼1.0 WAU·mg^{-1} protein (Fig. 3*B*, open bar). By contrast, cell lysate prepared from 1% CO_2-grown Pt43233:GFP1 cells displayed dramatically higher CO_2 hydration and HCO_3^- dehydration (Fig. 3*B*, closed bar), implying this additional CA activity was due to the overexpression of Pt43233.

Pt43233:GFP was immunoprecipitated from the Pt43233 overexpression line, Pt43233:GFP1, with anti-GFP antibody. Western blotting analysis of the protein-A Sepharose chromatography eluate revealed the presence of an 85-kDa polypeptide matching the predicted molecular mass of the Pt43233:GFP fusion protein (Fig. 3*C*). The final preparation was contaminated with the 50-kDa anti-GFP IgG. The specific CO_2 hydration activity of this partially purified Pt43233:GFP preparation was extremely high, whereas CA activity was not detected when the WT and Pt43233:GFP1 lysates were immunoprecipitated with anti-GFP IgG and nonimmune IgG, respectively (Fig. 3*D*).

Interestingly, the recombinant Pt43233 also displayed esterase activity (Fig. S5*B* and Table S1), which is a known characteristic of α- and δ-type CAs (21, 22). When *p*-nitrophenyl acetate was used as a substrate, Pt43233 contained an esterolysis specific activity of 773.9 ± 88.1 nmol·min^{-1}·mg^{-1} protein. The results of CA and esterase assays suggest that Pt43233 is a previously unidentified type of CA, classified as a θ type, albeit with enzyme characteristics similar to those enzyme characteristics apparent for α- and δ-type CAs.

Impacts of Overexpression and Silencing of Pt43233 on Growth and Photosynthesis. The separate impacts of an exogenously introduced Pt43233:GFP, driven by a fucoxanthin chlorophyll (Chl) *a*/*c* binding protein gene promoter (P*fcpA*), which is known to be a CO_2-independent promoter, and RNAi silencing of *Pt43233* on growth and photosynthesis were examined. Western blot analysis of cell lysates prepared from separate Pt43233:GFP transformants

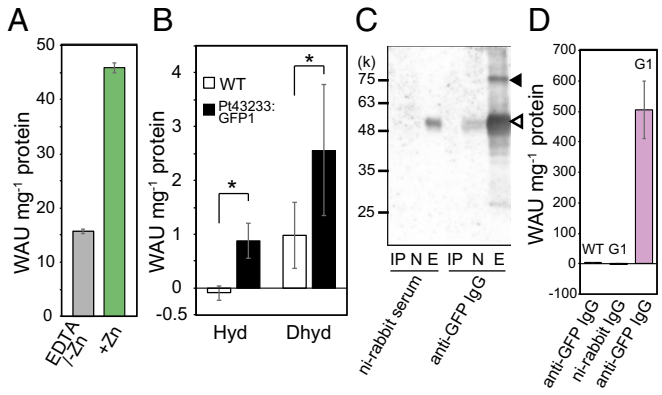

Fig. 3. CA activity of Pt43233. (*A*) CA activity of the purified recombinant Pt43233 in the absence (gray) and presence (green) of Zn. (*B*) CO_2 hydration (Hyd) and HCO_3^- dehydration (Dhyd) activities of cell lysates of WT (open bar) and Pt43233:GFP1 mutant (closed bars) grown under 1% CO_2. The result of the *t* test is indicated (*$P < 0.05$). (*C*) Western blot analysis of Pt43233:GFP following immunoprecipitation with anti-GFP antibody. E, eluted fraction; IP, input; N, nonbinding fraction; ni, nonimmune. The protein band corresponding to Pt43233:GFP is represented by the closed arrowhead, and the IgG protein band is represented by the open arrowhead. (*D*) CA activity of Pt43233:GFP immunoprecipitated with anti-GFP antibody. As a control, WT and Pt43233:GFP1 (G1) cell lysates were immunoprecipitated with anti-GFP IgG and nonimmune rabbit IgG, respectively. The error bar indicates the SD of three separate experiments.

(clones 1 and 2) revealed an immunoreactive 85-kDa protein, matching the predicted M_r of the fusion protein (Fig. S6*A*). RNAi suppression of *Pt43233* transcript levels in the *Pt43233*-i1 mutant was confirmed by RT-PCR (Fig. S6*B*); this mutant cell line was subjected to further experiments.

The growth characteristics of the Pt43233:GFP1 and *Pt43233*-i1 mutants were determined for cells cultured under air or 5% (vol/vol) CO_2. The pH of the medium in the high-CO_2 culture was in the range of 7.3–7.6, and it was in the range of 7.7–8.0 for air-cultured cells. The doubling rate of Pt43233:GFP1 cells was comparable to the doubling rate of WT cells, regardless of CO_2 conditions. By contrast, the doubling rates of *Pt43233*-i1 cells were 64% and 57% of WT cells cultured under 5% (vol/vol) CO_2 and air, respectively (Fig. 4*A* and Table 1), implying that *Pt43233* is pivotal for growth.

The impact of Pt43233 overexpression on photosynthetic parameters was determined for *P. tricornutum* cells cultured in standard seawater at pH 8.2. The DIC concentration to give one-half-maximum rate of photosynthesis ($K_{0.5}$[DIC]) of Pt43233:GFP1 cells decreased to 61% relative to WT cells when cultured under 5% (vol/vol) CO_2, although such a difference in photosynthetic parameters between Pt43233:GFP and WT cells was not observed when cultured in air (Fig. 4*B* and Table 1). This increase in photosynthetic affinity for DIC in 5% CO_2-grown Pt43233:GFP1 cells was associated with an increase in the apparent photosynthetic conductance (APC), which was twofold greater than the APC of WT cells (Table 1). Pt43233:GFP2 cells grown under 1% CO_2 rendered a $K_{0.5}$[DIC] value that was about 67% of the $K_{0.5}$[DIC] value apparent in WT cells under an assay condition at pH 7.5 (Table S2). These results suggest that overexpression of Pt43233 could confer a stimulated photosynthetic DIC affinity independent of assay pH on high-CO_2–grown cells whose endogenous biophysical CCM is largely suppressed (3, 23). In contrast, photosynthetic parameters were not affected by the overexpression of Pt43233:GFP in air-grown cells (Fig. 4*B* and Table 1).

The functional relevance of Pt43233 for photosynthetic efficiency was evaluated at a media pH of 8.2 in an experiment using *Pt43233*-i1 cells. $K_{0.5}$[DIC] in air-grown *Pt43233*-i1 cells had an approximate 4.5-fold higher value relative to WT cells, although little difference in $K_{0.5}$[DIC] was observed between high-CO_2–grown WT and *Pt43233*-i1 cells (Fig. 4*B* and Table 1). When grown under air, the maximum photosynthetic capacity (P_{max}) in *Pt43233*-i1 cells was reduced to 85% of the P_{max} detected in WT cells (Fig. 4*B* and Table 1). The APC of air-grown *Pt43233*-i1 cells was about 24% of the APC of WT cells (Table 1). These photosynthetic characteristics in *Pt43233*-i1 cells relative to the photosynthetic characteristics in WT cells were highly similar in a range of the assay pHs from 7.5 to 9.0 in cells grown under air condition (Table S2).

Discussion

The variation in the localization of CA within chloroplasts of *C. reinhardtii* and *P. tricornutum* has suggested fundamental differences in the function of the pyrenoids with respect to their DIC flux control mechanisms and mechanistic diversity in the algal CCM (7, 8). However, the biochemical and physiological investigations of Pt43233 revealed that the potential function of the pyrenoid-penetrating thylakoid in the final step of the CCM is consistent between freshwater green alga and marine diatoms, implying the function of CA in the thylakoid lumen to be a general mechanism in some algal CCMs and photosynthesis. In addition, this study strongly implies the convergent evolution of algal CCMs consisting of a wide spectrum of CCM components of diverse origins, culminating in a common DIC flux control system around RubisCO by using the pH environment of the thylakoid lumen. Biochemical characterization of Pt43233 revealed it to be a previously unidentified θ-CA, which is targeted to the lumen of the pyrenoid-penetrating thylakoid by an N-terminal signal sequence (Fig. 2 *I* and *J* and Fig. S2), suggesting its role is tightly associated with pyrenoid function.

CAs are known to contain divalent metal ions (usually Zn) at their active site, whereby Zn is coordinated to three histidines in α, γ-, and δ-CAs, whereas β- and ζ-CAs are bound to one histidine, two cysteines,; and sometimes an additional aspartate (24, 25). A η-CA in the malaria parasite, *Plasmodium falciparum*, has three histidines for Zn coordination and is phylogenetically related to α-CA (26). Apart from their CGHR domains, the four CGHR family factors in *P. tricornutum* are dissimilar to LCIB/D in *C. reinhardtii*. The detection of Zn in purified Pt43233 strongly suggests that at least three residues of the highly conserved CGHR domain residues in Pt43233, specifically Cys^{307}, Asp^{309}, His^{349}, His^{363}, and Cys^{387}, are responsible for Zn binding (Fig. 1*B*).

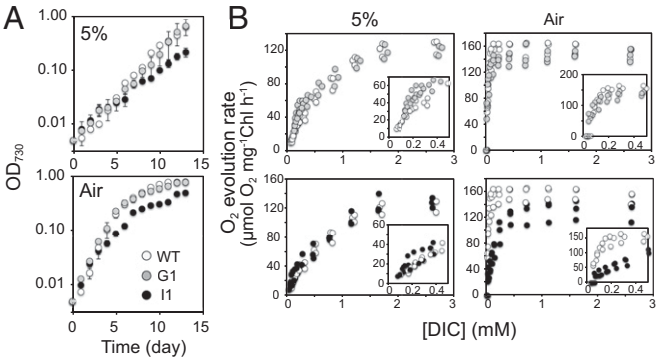

Fig. 4. Effect of Pt43233 overexpression and down-regulation on photosynthetic parameters and growth of *P. tricornutum*. (*A*) Growth curves of WT, Pt43233:GFP1 (G1), and *Pt43233*-i1 (I1) cells. Cells were cultured under 5% (vol/vol) CO_2 (5%) or 0.04% CO_2 (Air). Data represent mean ± SD of three separate experiments. (*B*) Kinetic plots of photosynthetic rate in WT, G1, and I1 cells cultivated under 5% (vol/vol) CO_2 (5%; *Left*) and 0.04% CO_2 (Air; *Right*). (*Insets*) Plots at low DIC concentrations. In all plots, open circles represent WT cells, closed gray circles represent G1 cells, and closed black circles represent I1 cells.

Table 1. Growth and photosynthetic characteristics in WT, Pt43233:GFP1, and *Pt43233*-i1 cells determined in the standard seawater pH (8.2)

CO_2	Cell	Doubling rate, times, d^{-1}	P_{max},* μmol O_2 mg^{-1} Chl h^{-1}	$K_{0.5}$[DIC],† μM	APC, μmol O_2 L·μmol^{-1} DIC mg^{-1} Chl h^{-1}
5% (vol/vol)	WT	0.64 ± 0.07	157.4 ± 11.2	697.3 ± 136.5	0.19 ± 0.08
	Pt43233:GFP1	0.52 ± 0.07	149.1 ± 1.6	428.5 ± 117.2	0.38 ± 0.13
	Pt43233-i1	0.41 ± 0.06	160.9 ± 15.9	757.7 ± 141.1	0.18 ± 0.15
Air	WT	0.92 ± 0.13	163.0 ± 0.9	36.0 ± 2.7	4.2 ± 0.7
	Pt43233:GFP1	0.80 ± 0.04	152.4 ± 7.6	30.6 ± 8.3	3.5 ± 0.9
	Pt43233-i1	0.52 ± 0.04	139.1 ± 19.3	168.9 ± 37.2	1.0 ± 0.4

All values are mean ± SD of the three separate experiments.
*Maximum photosynthetic rate.
†[DIC] to give half-maximum P_{max}.

Indeed, the presence of an active site coordinated Zn increased CA activity of Pt43233 (Fig. 3*A*). On the basis of putative active-site amino acids, θ-CA is dissimilar to α- and δ-CAs and most similar to β- and ζ-CAs, which use cysteine, histidine, and sometimes aspartate for Zn coordination (24, 25). By contrast, the recombinant Pt43233 exhibited esterase activity in addition to CA activity (Fig. S5*B* and Table S1). Esterase activity is well known for α- and δ-CAs, and together with the evidence for Zn binding to the active site, the biochemical properties of this θ-CA appear to be distinct from other known CAs.

The specific CA activity of the recombinant Pt43233 was low for this type of enzyme. The reason for this low activity is unclear, but it is possible that a posttranslational activation mechanism is required for maximum activity in diatom cells, such as redox modification, glycosylation, or phosphorylation, which could be absent in the recombinant protein produced in *E. coli* cells. In fact, immunoprecipitation of a Pt43233:GFP fusion protein from *P. tricornutum* transformants with anti-GFP antibody yielded a partially purified CA with a specific activity of 500 WAU·mg^{-1} protein (Fig. 3*D*). It is worth mentioning that the immunoprecipitated Pt43233:GFP-fusion protein preparation was contaminated with anti-GFP IgG (Fig. 3*C*); it is expected that final specific activity in a homogeneous preparation should be a few fold higher, approximating the specific activity known for α- and β-type CAs, measured at 900–6,500 WAU·mg^{-1} protein and 1,200 WAU·mg^{-1} protein, respectively (21, 27). Taken together, these results suggest that θ-CA activity is posttranslationally regulated in vivo. Such CA activation mechanisms are not without precedent, because the activity of CAH3, a thylakoid-luminal CA in *C. reinhardtii*, is regulated by phosphorylation (28).

Recent evidence points to the LCIB/C complex being localized around the pyrenoid in *C. reinhardtii*, and these proteins are postulated to be a part of a CO_2 recapturing system following leakage from the pyrenoid associated with the stromal β-CA, CAH6 (12). Alternatively, these proteins have been proposed to serve as components of the physical diffusion barrier against the CO_2 leakage (12, 29). This assumption is rational, given the spatial configurations of known CCM factors, specifically CAs that exist outside of the pyrenoid in *C. reinhardtii*. Furthermore, this DIC flux control system in *C. reinhardtii* is supported by a vast supply of CO_2 from the thylakoid-luminal α-CA, CAH3, which is promoted by luminal acidity under active photosynthesis (13, 15); no pyrenoidal CA has been described for *C. reinhardtii*. By contrast, the distribution of CA around the pyrenoid in marine diatoms does not fit the model described for the *Chlamydomonas*-type pyrenoid function; specifically, there is no thylakoidal CA or a free stromal CA in *P. tricornutum*, although pyrenoidal β-CAs, PtCA1 and PtCA2, do exist (8). However, the discovery of the θ-CA Pt43233 in the thylakoid lumen partially resolves this discrepancy regarding the location of biochemical and functional components associated with both CCMs. The direct utilization of the pH gradient across the thylakoid membrane yields an ample flux of CO_2 toward RubisCO, which could represent an essential evolutionary driving force for the functionality of the pyrenoid to ensure the efficient generation of CO_2 from HCO_3^- accumulated by algal biophysical CCMs. Although the origin of the components involved in this process appear to be extremely diverse and their physiological roles are inconsistent across CCM-using organisms, evolution may have strongly selected for this CCM system regardless of taxa and living environment.

Overexpression and knockdown mutants of Pt43233, respectively, culminated in the stimulation of photosynthetic efficiency at limited [DIC] conditions in high-CO_2–grown cells (Fig. 4*B*) and suppressed photosynthetic affinity in air-grown cells (Fig. 4*B*), and these phenotypes were stable over a range of assay medium pHs (Table 1 and Table S2). These results clearly demonstrate that the thylakoidal θ-CA participates in the supply of CO_2 to photosynthesis. Even though these phenotypic characteristics are more evident under limited DIC, the constitutive expression of Pt43233 (Fig. 2*K*) and the slower growth rate displayed in *Pt43233*-i1 mutant relative to WT cells under both high-CO_2 and air conditions (Fig. 4*A*) suggest a fundamental role of this luminal θ-CA in addition to the CCM, whereby it could stabilize the pH gradient and/or photosystem components by facilitating DIC/proton equilibrium in the thylakoid lumen. This potential dual functionality of the *P. tricornutum* luminal CA is similar to the dual functionality known for CAH3 in *C. reinhardtii*. The impairment of CAH3 in *C. reinhardtii* yields a high-CO_2-requiring phenotype, indicative of its pivotal function in the CCM (14, 30), but expression of CAH3 is constitutive and CAH3 might regulate PSII activity by removing a proton from the water-oxidizing complex (16, 17).

The precise mechanisms underlying the dual function of luminal CAs on CCM and PSII activity are not fully understood for algae. However, the physiological data in this study strongly suggest that Pt43233 is crucial for the generation of CO_2 flux toward RubisCO, presumably using (and/or regulating) the thylakoidal ΔpH. Thus, pyrenoidal PtCA1 and PtCA2 could have alternate functions apart from providing CO_2 to RubisCO from accumulated HCO_3^- in the pyrenoid (5, 6, 8). In a model of the CCM in *C. reinhardtii* proposed by Raven (15), thylakoid-based CO_2 formation requires HCO_3^- transport into the lumen. Thus, PtCA1 and PtCA2 could work in recapturing any leaked CO_2 to supply HCO_3^- to a putative transport system in the thylakoid membrane, although this transporter is yet to be discovered. The possibility also remains that the CGHR family in *C. reinhardtii*, specifically LCIB/C, could have CA activity. Under this scenario, the LCIB/C complex could support the CO_2-recapturing model of *C. reinhardtii* by converting leaking CO_2 into HCO_3^- at the peripheral pyrenoid area in the absence of functional association with stromal β-CA, CAH6.

In this study, the discovery of a thylakoid-luminal θ-CA in *P. tricornutum* indicates that the pyrenoid (thus, eukaryotic CCM) coevolved with the function of the thylakoid membrane regardless

of habitat and taxa. The marine centric diatom, *T. pseudonana*, also contains a CGHR factor with structural similarity to Pt43233 (Fig. S2*A*), suggesting that luminal θ-CA is a general feature of marine diatoms. Thylakoid-luminal CAs evolved from diverse origins across distant algal taxa, which strongly suggests that the thylakoid-based control system of DIC flux and DIC/proton balance was a pivotal driving force for the evolution of the photosynthetic mechanism in algae.

Materials and Methods

Cells and Culture Conditions. The marine diatom *P. tricornutum* Bohlin (UTEX642) was obtained from the University of Texas Culture Collection of Algae and grown in artificial seawater supplemented with one-half-strength Guillard's "F" solution (F/2ASW) (31) under continuous illumination (50–75 $\mu mol \cdot m^{-2} \cdot s^{-1}$) at 20 °C with atmospheric air (0.04% CO_2) or with elevated CO_2 [1% or 5% (vol/vol)].

Measurement of CA Activity. CA activity was measured as described by Wilbur and Anderson (32), with some modifications. Briefly, a 20-μL aliquot of CA solution was added to 1.48 mL of 20 mM barbital buffer (pH 8.4) in a water-jacketed acrylic chamber maintained at 2 °C. The CO_2 hydration reaction was initiated by the addition of 0.5 mL of ice-cold CO_2-saturated water, and the time required for the pH to drop from 8.3 to 8.0 was determined. Alternatively, 50 mM Mes·NaOH (pH 5.5) buffer with the addition of 0.5 mL of ice-cold 50 mM $NaHCO_3$, and the following pH increase from 5.7 to 6.0, was monitored for the HCO_3^- dehydration assay. The activity of CA was calculated as the WAU according to Eq. **1**:

$$WAU = T_0/T - 1, \quad [1]$$

where T_0 and T are the times required for the pH shift in the absence and the presence of CA, respectively.

Determination of Photosynthetic Parameters. Cultured cells were harvested by centrifugation at mid-logarithmic phase and washed with DIC-free F/2ASW (pH 7.5, 8.2, or 9.0). Cells were suspended in the DIC-free F/2ASW at a Chl *a* concentration of 10 $\mu g \cdot mL^{-1}$. The kinetics plot of the rate of photosynthetic O_2 evolution versus DIC concentration was based upon the value measured with a Clark-type oxygen electrode (3). The [DIC] at the CO_2 compensation point was measured by gas chromatography (3). $K_{0.5}$[DIC] and P_{max} values were determined by curve fitting with the nonlinear least squares method. The APC value was calculated from the initial slope of the kinetics plot.

Additional details on materials and methods are provided in *SI Materials and Methods*, and a list of primers is provided in Table S3.

ACKNOWLEDGMENTS. We thank Dr. Gale G. Bozzo for critical reading of this manuscript, Yukiko Yamazaki and Nobuko Higashiuchi for their technical assistance, and Miyabi Inoue for her skillful secretarial aid. This work was supported by Grant-in-Aid for Scientific Research B 24310015 (to Y.M.); Grant-in-Aid for Scientific Research on Innovative Areas 16H06557 (to Y.M.); Grants-in-Aid for Young Scientists B 15K21531 (to S.K.), 26870750 (to K.N.), and 15K16156 (to Y.T.) from the Japan Society for the Promotion of Science (JSPS); Science Research Promotion Fund Grant g135011 (to S.K.) from the Japan Private School Promotion Foundation; by the MEXT-supported program for the Strategic Research Foundation for the Advancement of Environmental Protection Technology and for Development of Intelligent Self-Organized Biomaterials; and by the PMAC-supported Science Research Promotion Fund (Y.M.).

1. Falkowski P, et al. (2000) The global carbon cycle: A test of our knowledge of earth as a system. *Science* 290(5490):291–296.
2. Field CB, Behrenfeld MJ, Randerson JT, Falkowski P (1998) Primary production of the biosphere: Integrating terrestrial and oceanic components. *Science* 281(5374): 237–240.
3. Matsuda Y, Hara T, Colman B (2001) Regulation of the induction of bicarbonate uptake by dissolved CO_2 in the marine diatom, *Phaeodactylum tricornutum*. *Plant Cell Environ* 24(6):611–620.
4. Nakajima K, Tanaka A, Matsuda Y (2013) SLC4 family transporters in a marine diatom directly pump bicarbonate from seawater. *Proc Natl Acad Sci USA* 110(5):1767–1772.
5. Hopkinson BM (2014) A chloroplast pump model for the CO_2 concentrating mechanism in the diatom *Phaeodactylum tricornutum*. *Photosynth Res* 121(2-3):223–233.
6. Hopkinson BM, Dupont CL, Allen AE, Morel FMM (2011) Efficiency of the CO_2-concentrating mechanism of diatoms. *Proc Natl Acad Sci USA* 108(10):3830–3837.
7. Samukawa M, Shen C, Hopkinson BM, Matsuda Y (2014) Localization of putative carbonic anhydrases in the marine diatom, *Thalassiosira pseudonana*. *Photosynth Res* 121(2-3):235–249.
8. Tachibana M, et al. (2011) Localization of putative carbonic anhydrases in two marine diatoms, *Phaeodactylum tricornutum* and *Thalassiosira pseudonana*. *Photosynth Res* 109(1-3):205–221.
9. Badger MR, Hanson D, Price GD (2002) Evolution and diversity of CO_2 concentrating mechanisms in cyanobacteria. *Funct Plant Biol* 29(2-3):161–173.
10. Kaplan A, Reinhold L (1999) CO_2 concentrating mechanisms in photosynthetic microorganisms. *Annu Rev Plant Physiol Plant Mol Biol* 50:539–570.
11. Ramazanov Z, et al. (1994) The induction of the CO_2-concentrating mechanism is correlated with the formation of the starch sheath around the pyrenoid of *Chlamydomonas reinhardtii*. *Planta* 195(2):210–216.
12. Yamano T, et al. (2010) Light and low-CO_2-dependent LCIB-LCIC complex localization in the chloroplast supports the carbon-concentrating mechanism in *Chlamydomonas reinhardtii*. *Plant Cell Physiol* 51(9):1453–1468.
13. Moroney JV, Ynalvez RA (2007) Proposed carbon dioxide concentrating mechanism in *Chlamydomonas reinhardtii*. *Eukaryot Cell* 6(8):1251–1259.
14. Funke RP, Kovar JL, Weeks DP (1997) Intracellular carbonic anhydrase is essential to photosynthesis in *Chlamydomonas reinhardtii* at atmospheric levels of CO_2. Demonstration via genomic complementation of the high-CO_2-requiring mutant *ca-1*. *Plant Physiol* 114(1):237–244.
15. Raven JA (1997) CO_2-concentrating mechanisms: A direct role for thylakoid lumen acidification? *Plant Cell Environ* 20(2):147–154.
16. Shutova T, et al. (2008) The photosystem II-associated Cah3 in *Chlamydomonas* enhances the O_2 evolution rate by proton removal. *EMBO J* 27(5):782–791.
17. Benlloch R, et al. (2015) Crystal structure and functional characterization of photosystem II-associated carbonic anhydrase CAH3 in *Chlamydomonas reinhardtii*. *Plant Physiol* 167(3):950–962.
18. Gruber A, et al. (2007) Protein targeting into complex diatom plastids: Functional characterisation of a specific targeting motif. *Plant Mol Biol* 64(5):519–530.
19. Ishida K, Green BR (2002) Second- and third-hand chloroplasts in dinoflagellates: Phylogeny of oxygen-evolving enhancer 1 (PsbO) protein reveals replacement of a nuclear-encoded plastid gene by that of a haptophyte tertiary endosymbiont. *Proc Natl Acad Sci USA* 99(14):9294–9299.
20. Supuran CT (2010) Carbonic anhydrase inhibitors. *Bioorg Med Chem Lett* 20(12): 3467–3474.
21. Lee RBY, Smith JAC, Rickaby REM (2013) Cloning, expression and characterization of the δ-carbonic anhydrase of *Thalassiosira weissflogii* (Bacillariophyceae). *J Phycol* 49(1):170–177.
22. Pocker Y, Sarkanen S (1978) Carbonic anhydrase: Structure catalytic versatility, and inhibition. *Adv Enzymol Relat Areas Mol Biol* 47:149–274.
23. Burkhardt S, Amoroso G, Riebesell U, Sültemeyer D (2001) CO_2 and HCO_3^- uptake in marine diatoms acclimated to different CO_2 concentrations. *Limnol Oceanogr* 46(6): 1378–1391.
24. Xu Y, Feng L, Jeffrey PD, Shi Y, Morel FM (2008) Structure and metal exchange in the cadmium carbonic anhydrase of marine diatoms. *Nature* 452(7183):56–61.
25. Mitsuhashi S, et al. (2000) X-ray structure of β-carbonic anhydrase from the red alga, *Porphyridium purpureum*, reveals a novel catalytic site for $CO(_2)$ hydration. *J Biol Chem* 275(8):5521–5526.
26. Supuran CT, Capasso C (2015) The η-class carbonic anhydrases as drug targets for antimalarial agents. *Expert Opin Ther Targets* 19(4):551–563.
27. Bayram E, Senturk M, Kufrevioglu OI, Supuran CT (2008) In vitro inhibition of salicylic acid derivatives on human cytosolic carbonic anhydrase isozymes I and II. *Bioorg Med Chem* 16(20):9101–9105.
28. Blanco-Rivero A, Shutova T, Román MJ, Villarejo A, Martinez F (2012) Phosphorylation controls the localization and activation of the lumenal carbonic anhydrase in *Chlamydomonas reinhardtii*. *PLoS One* 7(11):e49063.
29. Wang Y, Spalding MH (2014) Acclimation to very low CO_2: Contribution of limiting CO_2 inducible proteins, LCIB and LCIA, to inorganic carbon uptake in *Chlamydomonas reinhardtii*. *Plant Physiol* 166(4):2040–2050.
30. Karlsson J, et al. (1998) A novel α-type carbonic anhydrase associated with the thylakoid membrane in *Chlamydomonas reinhardtii* is required for growth at ambient CO_2. *EMBO J* 17(5):1208–1216.
31. Harrison PJ, Waters RE, Taylor FJR (1980) A broad-spectrum artificial seawater medium for coastal and open ocean phytoplankton. *J Phycol* 16(1):28–35.
32. Wilbur KM, Anderson NG (1948) Electrometric and colorimetric determination of carbonic anhydrase. *J Biol Chem* 176(1):147–154.
33. Guindon S, et al. (2010) New algorithms and methods to estimate maximum-likelihood phylogenies: Assessing the performance of PhyML 3.0. *Syst Biol* 59(3):307–321.
34. Kitao Y, Harada H, Matsuda Y (2008) Localization and targeting mechanisms of two chloroplastic beta-carbonic anhydrases in the marine diatom *Phaeodactylum tricornutum*. *Physiol Plant* 133(1):68–77.
35. Fu G, Nagasato C, Oka S, Cock JM, Motomura T (2014) Proteomics analysis of heterogeneous flagella in brown algae (stramenopiles). *Protist* 165(5):662–675.